RSC Advances

PAPER

View Article Online
View Journal | View Issue

Cite this: *RSC Adv.*, 2024, **14**, 2182

Horseradish peroxidase-catalyzed polyacrylamide gels: monitoring their polymerization with BSA-stabilized gold nanoclusters and their functional validation in electrophoresis†

Chang Liao,‡[a] Tao Li,‡[a] Fengjiao Chen,[b] Shaoying Yan,[c] Liying Zhu,[d] Hua Tang *[a] and Dan Wang *[e]

Polyacrylamide gel (PAG) is extensively used as a matrix for biomolecular analysis and fractionation. However, the traditional polymerization catalyst system *N*,*N*,*N*′,*N*′-tetramethylethylenediamine (TEMED)/ammonium persulphate (APS) of PAG presents non-negligible toxicity. Herein, we utilized the green and efficient bio-enzyme horseradish peroxidase (HRP) to catalyze the gel polymerization of polyacrylamide. At the same time, the efficacy of this gel system in separating nucleic acids and proteins was confirmed by applying the gel system in electrophoresis. This study aims to explore a higher biosafety polyacrylamide gel polymerization catalytic system which can be applied to electrophoresis technology. Furthermore, in order to differentiate between the bio-enzymatic catalytic system and the traditional toxic catalytic system during polymerization, aggregation-induced luminescence (AIE) of bovine serum albumin-stabilized gold nanoclusters (BSA-Au NCs) was used to monitor the polymerization reaction of the system. The results indicated that the fluorescence intensity of the polymeric system containing BSA-Au NCs increased with the polymerization of the monomers. Subsequently, we assessed whether certain components of nucleic acid electrophoresis and protein electrophoresis such as sodiumdodecylsulfate (SDS) and TBE buffer (Tris-boric acid, EDTA, pH 8.3) would affect the polymerization of the polyacrylamide gels catalyzed by the biological enzymes. The experimental conditions were also optimized to explore the optimal concentration of the ternary system of HRP, H_2O_2 and ACAC. Our results suggested that the bioenzyme-catalyzed system could be a feasible alternative to the TEMED/APS-catalyzed system, which also could provide new insights into the methods of monitoring the polymerization system.

Received 23rd October 2023
Accepted 24th December 2023

DOI: 10.1039/d3ra07208h

rsc.li/rsc-advances

Introduction

Polyacrylamide gel electrophoresis (PAGE) is a method of electrophoresis with polyacrylamide gel as support, which provides a versatile method for analysis and characterization of proteins and nucleic acids.[1–3] Polyacrylamide gel is a three-dimensional gel with a network-like structure that formed through the polymerization and cross-linking of acrylamide and *N*,*N*′-methylenebisacrylamide (Acr-Bis), catalyzed by *N*,*N*,*N*′,*N*′-tetramethylethylenediamine/ammonium persulphate (TEMED/APS).[4,5] However, the potential toxicity of APS and TEMED restricts their usage in the field of biology. It is widely acknowledged that APS has the tendency to induce various cutaneous and respiratory reactions, such as irritant dermatitis, localized edema, urticaria, rhinitis, and asthma.[6–9] In addition, TEMED irritates the skin, eyes and respiratory tract, which is also toxic to the brain by inhibiting acetylcholinesterase and has intensive neurotoxic effects.[10,11] Consequently, it is extremely necessary to explore a safe catalytic system for gel polymerization. Bioenzyme-mediated radical polymerization was firstly reported by Parravano in 1951.[12] Extensive research has shown that enzymatic polymerization is a friendly strategy for the preparation of mechanically robust nanocomposite hydrogels.[13–17] HRP is a very popular and efficient bioenzyme that has been researched in the preparation of hydrogel.[18–20] In 1992, Derango *et al.* conducted an initial study that demonstrated the application of HRP and other

[a]*Key Laboratory of Molecular Biology for Infectious Diseases (Ministry of Education), Chongqing Medical University, Chongqing 400016, China. E-mail: tanghua86162003@cqmu.edu.cn; cqwangdan61@163.com*

[b]*Guangshan County People's Hospital, Xinyang 465450, China*

[c]*Department of Clinical Laboratory, The First Affiliated Hospital of Nanchang University, Nanchang, Jiangxi 330000, China*

[d]*Center for Clinical Laboratories, Affiliated Hospital of Guizhou Medical University, Guiyang 550004, China*

[e]*Post-Doctoral Research Center, The People's Hospital of Rongchang District, Chongqing 402460, China*

† Electronic supplementary information (ESI) available. See DOI: https://doi.org/10.1039/d3ra07208h

‡ Chang Liao and Tao Li have contributed equally to this work.

oxidase enzymes as catalysts for the polymerization of vinyl monomers by free radicals.[21] Subsequently, Su *et al.* reported that the polymerization of hydrogels was initiated by ACAC radicals derived from the HRP/H_2O_2/ACAC ternary system. Within this ternary system, HRP serves as the initiator for the polymerization of acrylamide monomer by catalyzing H_2O_2 to produce $OH^{\bullet}$, and then oxidizes ACAC to form $ACAC^{\bullet}$.[22] Inspired by these pioneering studies, we propose the utilization of the HRP/H_2O_2/ACAC ternary system as an alternative to TEMED/APS for catalyzing the polymerization of Acr-Bis.

The role of monomer and catalyst diffusion in the kinetics of polymerization is significant. In order to comprehensively comprehend the disparities in monomer polymerization initiated by these two systems, it is beneficial to monitor the polymerization process *in situ*. However, current monitoring techniques for free radical polymerization require the use of special instruments such as rheometers, viscometers or nuclear magnetic resonance (NMR).[23,24] Fluorescence is an ideal tool in this field due to its high sensitivity.[25,26] Since most polymers exhibit weak fluorescence or non-fluorescence, doping an external fluorescent dye to monitor the polymerization reaction is necessary. In 2001, Tang *et al.* made a significant finding that a group of TPS molecules exhibit a lack of light emission in solution, but demonstrate luminescence when aggregated. These molecules were subsequently termed AIE reaction molecules.[27–29] The unrestricted movement of AIE molecules in solution leads to the conversion of light energy into thermal energy dissipation, resulting in the quenching of fluorescence. However, in the aggregated state, where intramolecular motion is constrained, the non-radiative decay process of the excited state is impeded, leading to a decrease in the proportion of energy dissipated through motion. Hence, the fluorescence exhibited by AIE luminescent groups is highly responsive to alterations in the surrounding environment. Previous studies have demonstrated the presence of AIE effect in Au NCs.[30–32] Given the substantial increase in viscosity following gel polymerization, the AIE effect of Au NCs can effectively reflect this transformation, thereby enabling the monitoring of gel polymerization. Nevertheless, the hydrophobic nature of Au NCs restricts their functionality within hydrogels. Au NCs, which are stabilized by diverse ligands, exhibit exceptional water solubility and their AIE properties have found extensive applications.[33–35] BSA-Au NCs have demonstrated notable merits in direct synthesis, biocompatibility, low toxicity, and exceptional photostability.[36,37] Consequently, we employed BSA-Au NCs to monitor the gel polymerization process. Our experimental findings indicated that the effectiveness of BSA-Au NCs in monitoring gel polymerization was consistent with the effect of NMR, affirming the feasibility of their utilization. To our knowledge, there has been no prior research on the utilization of BSA-Au NCs for monitoring polymerization reactions.

In this study, we had innovatively employed the environmentally friendly HRP/H_2O_2/ACAC ternary initiating system as an alternative to the TEMED/APS system for initiating the polymerization of Acr-Bis. The process of Acr-Bis monomer polymerization initiated by HRP/H_2O_2/ACAC was depicted in Scheme 1A. To investigate the influence of two initiator systems on the formation of polyacrylamide gel, BSA-Au NCs with AIE characteristics were introduced into the polymerization system for real-time monitoring. Following gel polymerization, BSA-Au NCs exhibited a significant increase in fluorescence intensity when excited at a wavelength of 370 nm (Scheme 1B). These findings demonstrated that HRP/H_2O_2/ACAC could effectively initiate monomer polymerization within a short time, making it suitable for subsequent electrophoresis applications. This study presents an innovative proposal suggesting the use of non-toxic HRP/H_2O_2/ACAC as a replacement for the highly toxic TEMED/APS in order to facilitate the formation of polyacrylamide gel, while ensuring no adverse effects on subsequent nucleic acid and protein electrophoresis. Additionally, the polymerization of monomers can be effectively monitored through the AIE property of BSA-Au NCs.

Materials and methods

Materials and reagents

30% acrylamide (acrylamide/bisacylamide = 29 : 1), ammonium persulfate (APS) and 10% sodiumdodecylsulfate (SDS) were purchased from Wuhan Servicebio Technology Co., Ltd (Wuhan, China). 1 M Tris–HCl (pH 8.8) and 1 M Tris–HCl (pH 6.8) were bought from Beijing Labgic Technology Co., Ltd (Beijing, China). Chloroauric acid ($HAuCl_4$) and sodium hydroxide (NaOH) were supplied from Sinopharm Chemical Reagent Co., Ltd. (Shanghai, China). HRP (Rz > 3.0) was obtained from Sangon Biotechnology Co., Ltd (Shanghai, China). *N*,*N*,*N*′,*N*′-TEMED was purchased from Shanghai Aladdin Biochemical Technology Co., Ltd. Methanol was purchased from Chongqing Chuandong Chemical (GROUP) Co., Ltd (Chongqing, China). Coomassie blue staining solution and corresponding destaining solution were purchased from Beijing Leagene Biotech. Co., Ltd (Beijing, China). BSA was purchased from Dalian Meilun Biotech Co., Ltd (Dalian, China). Mouse anti-human β-actin antibody (mAbcam 8226) and goat anti-mouse IgG antibody conjugated to HRP (ab205719) were purchased from Abcam (Shanghai, China). Multicolor prestained protein ladder and goldview were purchased from Shanghai Epizyme Biomedical Technology Co., Ltd. DL500 DNA Marker was purchased from TAKARA Biotechnology Co., Ltd (Dalian, China). All of the reagents and chemicals used were of analytical reagent grade.

Apparatus

PAGE was performed on a DYY-6C electrophoresis analyzer (Liuyi Instrument Company, China) and imaged on a Bio-rad ChemDoc XRS (Bio-Rad, USA). The fluorescence kinetics were collected on the Synergy H1 Multi-Mode Reader (BioTek, USA). Ultraviolet-visible (UV-Vis) spectra of BSA-Au NCs was obtained with a UV-2550 UV-Vis spectrophotometer (Shimadzu, Japan). Fluorescence spectra of BSA-Au NCs was recorded using a Cary Eclipse fluorescence spectrophotometer (Agilent Technologies, USA). BSA-Au NCs in aqueous solution and mixed in polyacrylamide gel were identified by high-resolution transmission electron microscopy (HRTEM; FEI Tecnai G2 F20 S-Twin, USA). ^{1}H NMR spectra was recorded using a Bruker AVIII 600 MHz (Germany) at 25 °C.

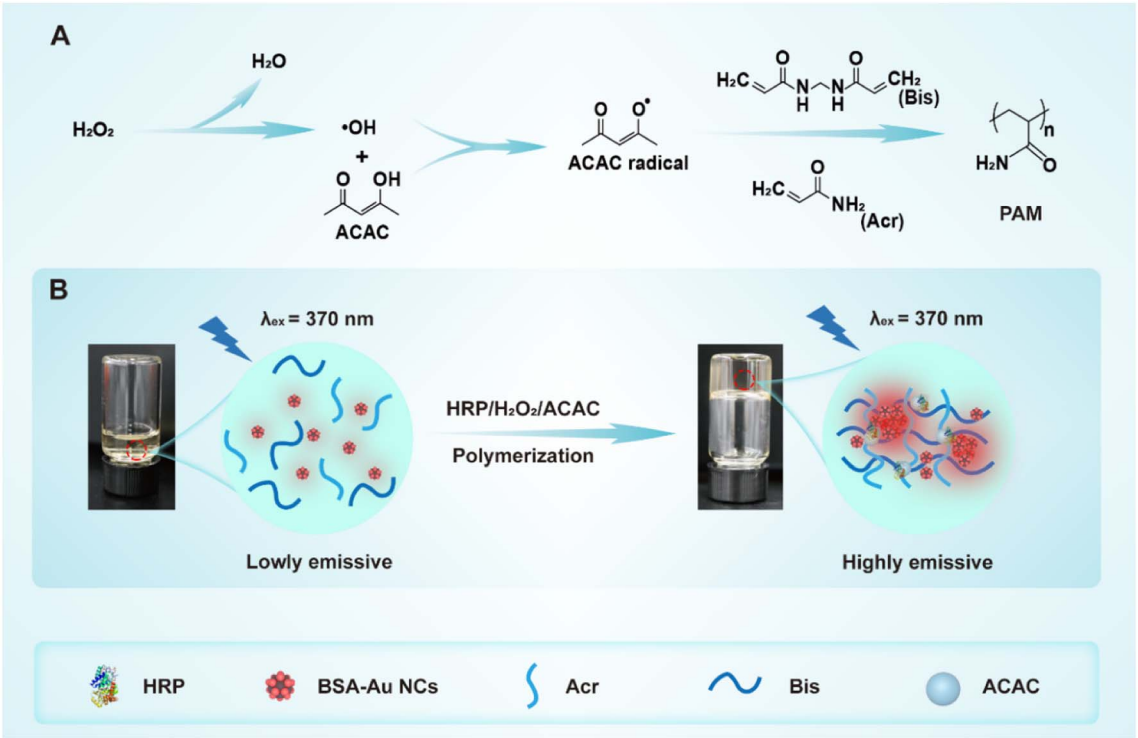

Scheme 1 Schematic illustration of (A) Acr-Bis polymerization catalyzed by HRP/H_2O_2/ACAC ternary initiation system and (B) the polymerization of Acr-Bis causes AIE phenomenon of BSA-Au NCs.

Preparation of BSA-Au NCs

According to prior methods,[38] aqueous $HAuCl_4$ solution (170 μL, 29.4 mM) was added to BSA solution (500 μL, 50 mg mL^{-1}) and reacted for 3 min, followed by the addition of NaOH (50 μL, 1 M) solution and reacted under vigorous stirring for 7 min, and incubated at 38 °C for 12 h. Then, the as-prepared BSA-Au NCs was filtered with a 3.5 kDa dialysis membrane. Next, the size, shape and optical properties of the synthetic BSA-Au NCs were characterized by HRTEM, UV-Vis absorption spectroscopy and laser emission spectroscopy, respectively. Finally, the prepared BSA-Au NCs were stored at 4 °C for further use.

Monitoring the polymerization reaction of Acr-Bis

Acr-Bis (330 μL), H_2O (550 μL) and BSA-Au NCs (100 μL) were mixed under vigorous vortex to give a homogenous solution. Then, initiating system of HRP (1 μL, 100 μg mL^{-1})/H_2O_2 (1 μL, 1 M)/ACAC (20 μL) or TEMED (1 μL)/APS (10 μL) were added into above mixed solution. After mixing, 200 μL of the mixture was added to a 96-well plate for detection immediately. The excitation wavelength was measured at 370 nm, and the emission wavelength was measured at 430 nm.

Native polyacrylamide gel electrophoresis (native-PAGE) of nucleic acids

10% native polyacrylamide gels catalyzed by HRP/H_2O_2/ACAC or TEMED/APS were prepared. DNA markers were then added to lanes for electrophoresis in 1 × TBE buffer (Tris-boric acid, EDTA, pH 8.3) at a constant voltage of 110 V for 45 min. Finally, the gels were stained with GelRed nucleic acid dye for 25 min and imaged by a gel image system.

PAGE of proteins

SDS-polyacrylamide gels (10% separation gel, 5% concentrated gel) catalyzed by TEMED/APS or HRP/H_2O_2/ACAC catalytic systems were prepared. Different concentrations of protein markers were then added to lanes for electrophoresis in tris-glycine running buffer. Gels were run at 80 V constant voltage for 30 min and 120 V for 60 min, respectively. Then the gels were stained using Coomassie Brilliant Blue for another 10 min, followed by destaining. These images were acquired by HUAWEI P40.

Western blot analysis

The total protein of MDA-MB-231 cells (Human breast cancer MDA-MB-231 cell line) was extracted and β-actin was used as a template. Then, the stacking and separating gels catalyzed by APS/TEMED or HRP/H_2O_2/ACAC were prepared, respectively. Prior to electrophoresis, the protein samples were heated in sample buffer (1 × loading buffer) for 10 min in a boiling water bath. After that, protein samples were loading into the individual wells, and electrophoresis. The separated proteins were blotting to PVDF membranes by electrotransfer, followed by incubated with primary antibodies (mouse anti-human β-actin antibody) and subsequently with the secondary antibody (goat anti-mouse IgG antibody). Finally, signals were detected with a ChampChemi imaging system (Beijing Sage Creation Science, Beijing, China).

Results and discussion

Characterization of BSA-Au NCs

Previous literatures had demonstrated the utilization of BSA for the stabilization and reduction of gold precursors *in situ*, resulting in the preparation of BSA-Au NCs with high quantum yields.[39–45] As shown in Fig. 1A, the prepared BSA-Au NCs showed dual emission wavelengths of 437 nm and 667 nm upon excitation at 368 nm. The UV-Vis absorption spectrum indicated that the synthesized BSA-Au NCs had no absorption peak at 520 nm, which meaned that the generation of Au NCs rather than gold nanoparticles (Fig. 1B).[46] The HRTEM images revealed a relatively uniform characteristic pattern of Au NCs with an average diameter of 2 ± 0.6 nm (Fig. 1C). Fig. 1D displayed the fluorescence decay curves of the BSA-Au NCs solution at 670 nm, as well as the quantum yield of the BSA-Au NCs solution at 400–700 nm (excitation at 380 nm). The average fluorescence lifetime of the BSA-Au NCs was determined to be 1.42 μs, and the photoluminescence quantum yield (PLQY) was approximately 10.57%, which aligned with previous findings.[47,48] The broad peak at 3284 cm^{-1} was due to the stretching of amino group (NH_2). The peaks located at 2960 cm^{-1} and 1169 cm^{-1} correspond to C–H and C–N stretching frequencies, respectively. The sharp peak located at 1637 cm^{-1} was attributed to the C=O stretching vibration, and the amide-amido (II) peak located at 1526 cm^{-1} was derived from peptide bonds in BSA. When BSA acted as a protective ligand for the formation of Au NCs, the characteristic peaks of the infrared spectra of BSA-Au NCs were slightly increased in comparison, which might be caused by the cluster formation (Fig. 1E). This was congruous with other reports in the literature.[49,50] We next examined the zeta potentials of the BSA solution and the BSA-Au NCs solution (Fig. 1F). The results showed that the zeta potential of those were close to each other, and the negative potential of the BSA-Au NCs increased. This was close to previous results in the literature.[51,52] Furthermore, Fig. S1† showed the TGA curves obtained for the BSA and the BSA-Au NCs at a temperature increase rate of 10 °C min^{-1}. The weight decreases of BSA and BSA-Au NCs occurred at the early stage close to 100 °C, and the loss was due to the bound water in the compounds. The BSA started to lose weight at 179 °C, indicating decomposition was occurring. The maximum weight loss occurred at 313 °C, which indicated that the decomposition rate had reached its maximum value. BSA-Au NCs showed the same weight reduction trend as BSA. These results indicated that the weight loss of BSA was greater than that of BSA-Au NCs, highlighting the formation of BSA-Au NCs. Fig. S2† showed XRD of BSA and BSA-Au NCs to determine the structure of BSA-Au NCs. Unfortunately, the simple XRD patterns of the prepared lyophilized powders prevented us from obtaining detailed structural information on the BSA-Au NCs. The crystallinity and diffraction angles of the synthesized BSA-Au NCs were examined in the

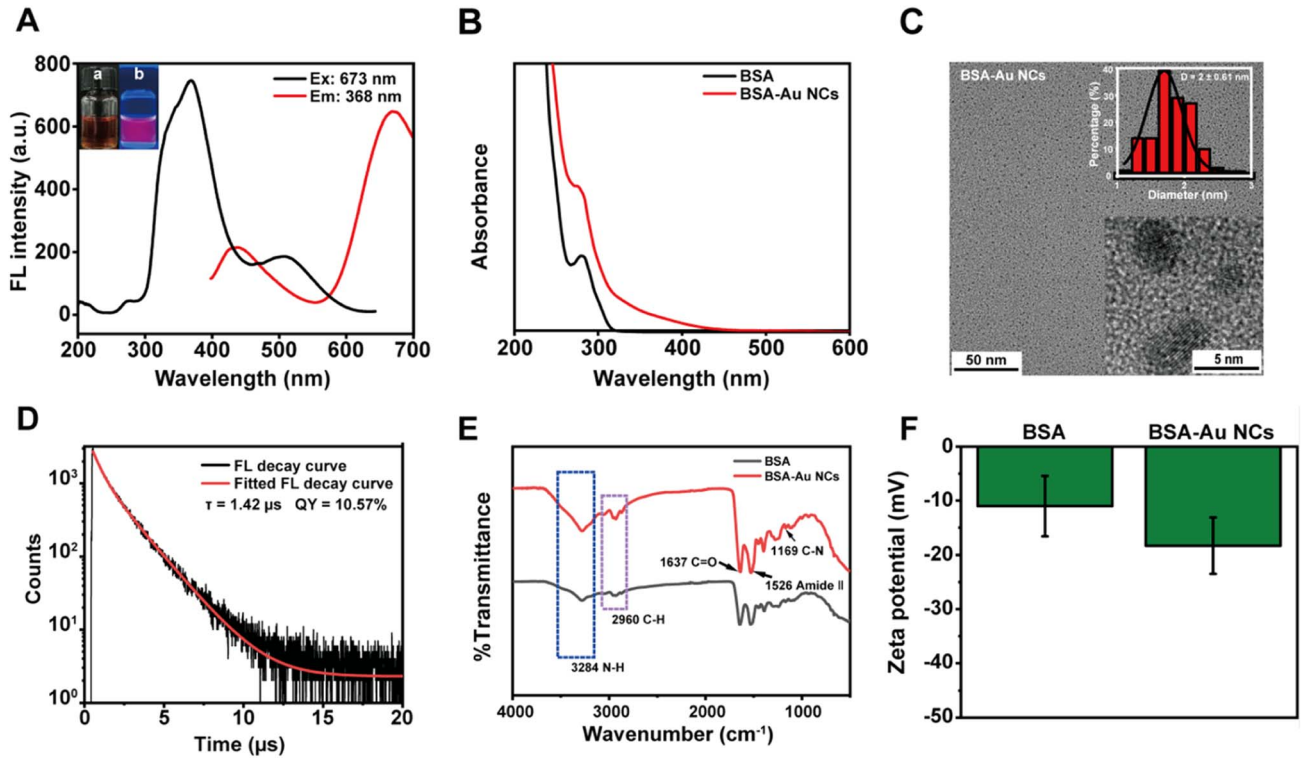

Fig. 1 **Characterization of BSA-Au NCs.** (A) The fluorescence spectrum of BSA-Au NCs. The inset displays the photographic images of BSA-Au NCs taken under daylight (a, ambient light) and UV light (b, 365 nm). (B) UV-visible absorption spectrum of BSA-Au NCs (red line) and BSA (black line). (C) HRTEM images of BSA-Au NCs. (D) Fluorescence decay profiles of BSA-Au NCs solution at 670 nm and quantum yield of BSA-Au NCs solution at 400–700 nm (excitation at 380 nm). (E) FT-IR spectrum of BSA (black line) and BSA-Au NCs (red line). (F) Zeta potential of BSA and BSA-Au NCs.

range of 10 to 90°. Referring to the Au standard card (PDF No. 04–0784), the BSA-Au NCs didn't have the needle-like diffraction peaks of the gold-based nanomaterials, and there was only a broad peak at 19°. This might be due to the Au atoms were mainly present in the form of Au clusters, which was consistent with previous literature.[53] These results provided evidence of the successful synthesis of BSA-Au NCs.

AIE effect of BSA-Au NCs in polyacrylamide gel

The proposal of embedding Au NCs into nano- or microporous nanomaterials, such as metal–organic frameworks, to achieve AIE luminescence through spatial confinement effects had inspired our investigation into inducing the AIE effect by doping Au NCs in polyacrylamide gel.[54] A significant enhancement in the fluorescence intensity of BSA-Au NCs was observed in polyacrylamide gels catalyzed by both catalytic systems, when compared to free BSA-Au NCs in Acr-Bis solution (Fig. 2A). Subsequently, an additional experiment was conducted to further investigate this phenomenon. The fluorescence intensity of both free BSA-Au NCs and aggregated BSA-Au NCs in the gel, exposed to UV light, was observed (Fig. S3†). It was found that BSA-Au NCs in the aggregated state exhibited significantly stronger fluorescence, which could be attributed to the AIE effect. The aggregation of BSA-Au NCs primarily occurred within the hydrogel (Fig. S4†). The XRD results of the two gels indicated the formation of an amorphous substance, which was characteristic of polyacrylamide and consistent with other reports in the literature.[55] The consistent FT-IR profiles also suggested that HRP/H_2O_2/ACAC could catalyze the formation of polyacrylamide gel (Fig. S5†). The AIE effect of BSA-Au NCs within the polyacrylamide gel was summarized schematically in Fig. 2B. The polymerization of the gel induced an increase in local viscosity, resulting in a significant fluorescence enhancement of BSA-Au NCs. Therefore, we proposed utilizing the AIE property of BSA-Au NCs to monitor the polymerization reaction of monomers. The fluorescence kinetic changes of Acr-Bis polymerization catalyzed by TEMED/APS or HRP/H_2O_2/ACAC were presented in Fig. 2C and F, respectively. The result demonstrated a gradual increase in fluorescence intensity over time during the gel polymerization process. In order to investigate the correlation between fluorescence intensity and monomer conversion rate, the change in monomer conversion over time in the polymerization system catalyzed by two initiator systems was characterized using ^{1}H-NMR spectroscopy (Fig. 2D, G and S6, S7†). These results showed that the enzyme-catalyzed polyacrylamide gel also had a high conversion rate. Remarkably, it was observed that monomer conversion exhibited an exponential relationship with photoluminescence (PL) intensity (Fig. 2E and H), suggesting a similar trend in variation between fluorescence intensity and monomer conversion. These findings indicated that the change in fluorescence intensity of BSA-Au NCs could be used as an indicator of the degree of polymerization of polyacrylamide gel. Furthermore, the fluorescence intensity of BSA-Au NCs increased as the polyacrylamide gel solidifies, providing further evidence that the AIE effect of BSA-Au NCs in gels could serve as probes to detect changes in viscosity during the polymerization process. SEM showed that both the two gels had a porous three-dimensional structure. The HRP/H_2O_2/ACAC-catalyzed polyacrylamide gel had a larger pore size compared to the conventional polyacrylamide gel (Fig. 2I and J). This result agreed with the monomer conversion rates of the two gels, with the larger pore size of the HRP/H_2O_2/ACAC-catalyzed gel corresponding to a lower monomer conversion rate. The TGA curves showed that the weight loss trend of the two gels was the same, while the weight loss ratio of HRP/H_2O_2/ACAC-catalyzed polyacrylamide gel was higher than that of TEMED/APS-catalyzed polyacrylamide gel (Fig. 2K). This might be due to the lower monomer conversion rate of the HRP/H_2O_2/ACAC-catalyzed gel, which meaned that more monomers were decomposed at a faster rate.

Optimization of experimental conditions

Prior to conducting the electrophoresis experiment, it is necessary to investigate whether certain components of nucleic acid and protein electrophoresis have an impact on the polymerization of Acr-Bis catalyzed by HRP/H_2O_2/ACAC. As shown in Fig. 3A, the observed changes in both the control group (black line) and the treatment group were found to be consistent. This consistency suggested that various factors within the reaction system, such as pH value, buffer solution and SDS, did not exert any significant influence on the polymerization reaction. Previous studies have reported that HRP possesses the ability to initiate the polymerization of Acr through catalyzing the oxidation of ACAC by H_2O_2.[56,57] We then proceeded to individually optimize the concentrations of ACAC, HRP, and H_2O_2 in order to determine an appropriate solidification time. The polymerization of the reaction system could be caused by the concentration of ACAC from 4.88 to 29.25 mg mL^{-1}, when using a fixed HRP concentration of 0.1 mg mL^{-1} and H_2O_2 concentration of 1.0 mM (Fig. 3B). From this, a concentration of 4.88 mg mL^{-1} was identified as the optimal concentration of ACAC for further experimentation and optimization. The impact of HRP on the polymerization of Acr-Bis was demonstrated in Fig. 3C. It was observed that a low concentration of HRP (0.01 mg mL^{-1}) did not result in an increase in fluorescence intensity, indicating that a low concentration of HRP was insufficient to facilitate the complete polymerization of Acr-Bis. Therefore, a concentration of 0.02 mg mL^{-1} HRP was selected. Subsequently, we explored the influence of H_2O_2 on gel polymerization. Fig. 3D demonstrated that the fluorescence intensity of the system containing a low concentration of H_2O_2 (0.1 mM) exhibited a slower increase, suggesting incomplete polymerization of Acr-Bis. Consequently, 0.5 mM H_2O_2 was chosen as the optimal concentration to ensure polymerization of the monomers within approximately 10 minutes.

Validation of the function of polyacrylamide gel initiated by HRP/H_2O_2/ACAC

Further verification is required to determine the impact of HRP-induced polymerization of Acr-Bis monomers on the electrophoretic function. The gel initiated by HRP/H_2O_2/ACAC system effectively distinguished DNA chains with varying molecular weights, similar to the traditional approach (Fig. 4A). Given that the protein marker is composed of proteins of varying sizes, it

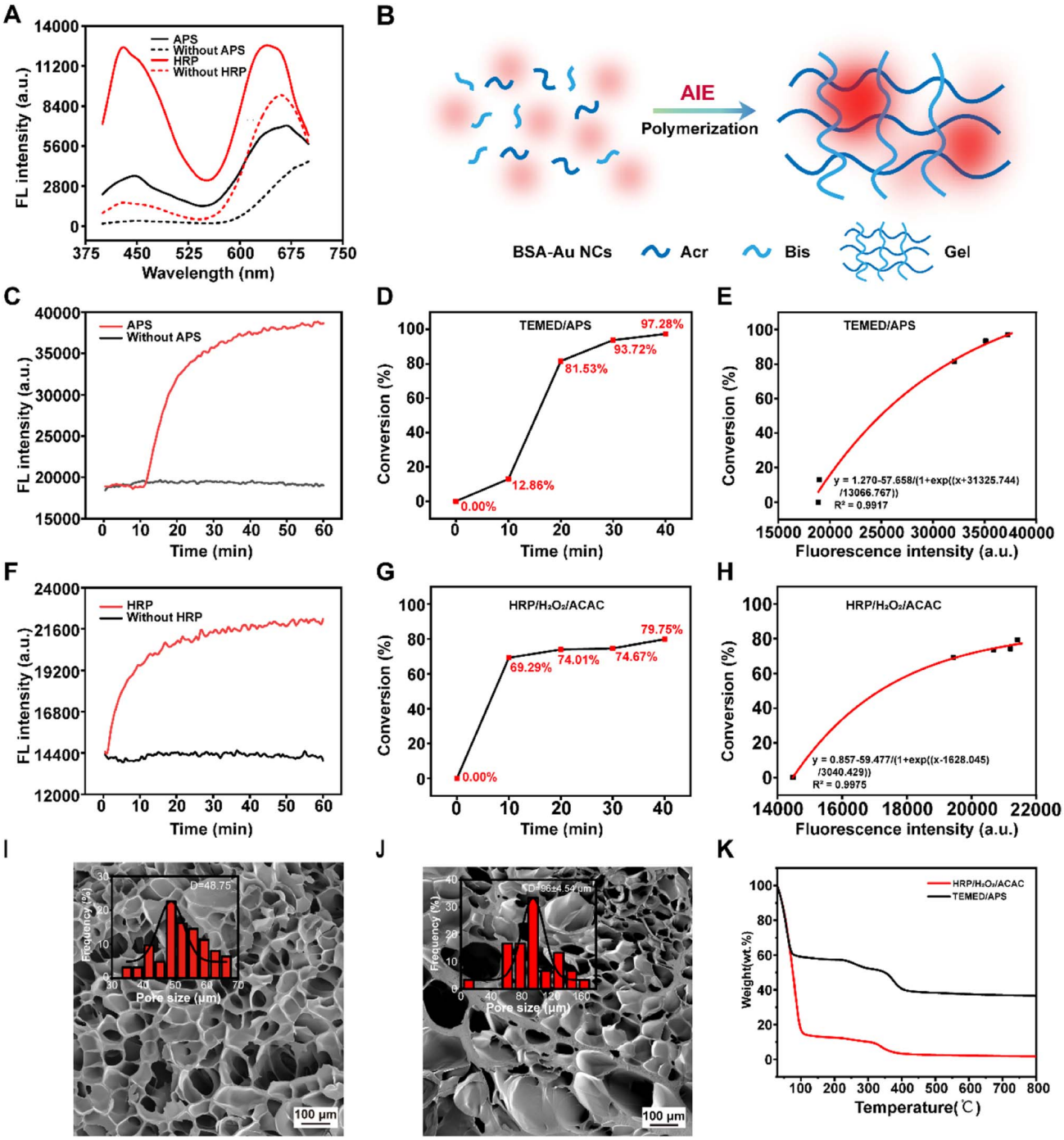

Fig. 2 **Identification of AIE effect of BSA-Au NCs in polyacrylamide gel.** (A) Fluorescence spectra of BSA-Au NCs before and after polymerization in a polyacrylamide gel catalyzed by TEMED/APS (black line) and HRP/H_2O_2/ACAC (red line). (B) Schematic Illustration of AIE effect of BSA-Au NCs in polyacrylamide gel. (C) The fluorescence kinetics of the polymerization system containing BSA-Au NCs catalyzed by TEMED/APS. (D) The monomer conversion of TEMED/APS initiated polymerization system at different time points. (E) The exponential relationship of conversion with PL intensity catalyzed by TEMED/APS. (F) The fluorescence kinetics of the polymerization system containing BSA-Au NCs catalyzed by HRP/H_2O_2/ACAC. (G) The monomer conversion of HRP/H_2O_2/ACAC initiated polymerization system at different time points. (H) The exponential relationship of conversion with PL intensity catalyzed by HRP/H_2O_2/ACAC. (I) SEM image of TEMED/APS-catalyzed polyacrylamide gels. (J) SEM image of HRP/H_2O_2/ACAC-catalyzed polyacrylamide gels. (K) TGA curves of polyacrylamide gels catalyzed by TEMED/APS and HRP/H_2O_2/ACAC.

serves as an indicator for discerning protein bands of different sizes. Consequently, we opted to employ the protein marker to assess the efficacy of the two gel systems in separating proteins of varying sizes. As depicted in Fig. 4B, the conventional gel exhibited proficient discrimination of small molecules, whereas the innovative gel demonstrated superior discrimination of

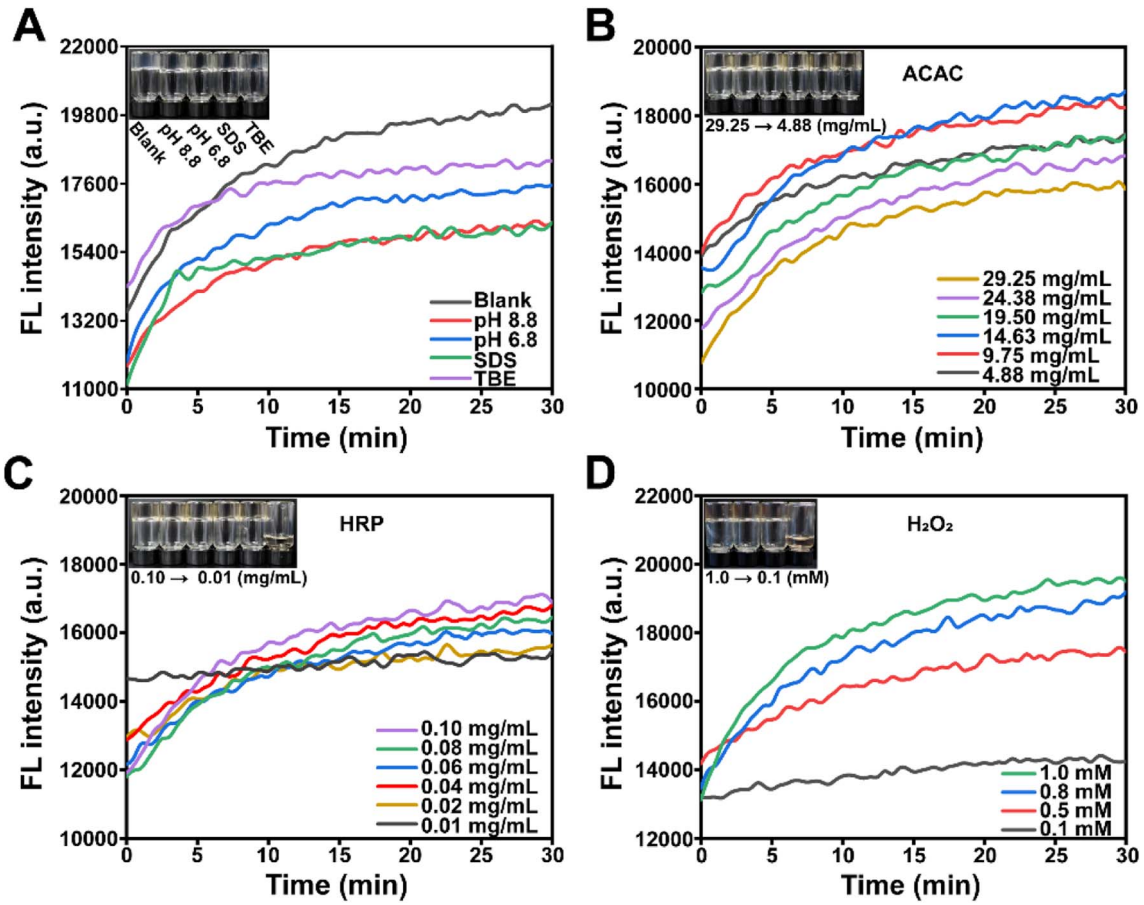

Fig. 3 **The optimization of experimental conditions.** (A) Effect of pH, SDS and TBE on gel polymerization. Inset: photographs of the polymerization system in response to different electrophoresis conditions. (B) Effect of ACAC concentration on gel polymerization. Inset: photographs of the polymerization system in response to different concentration of ACAC. (C) Effect of HRP concentration on gel polymerization. Inset: photographs of the polymerization system in response to different concentration of HRP. (D) Effect of H_2O_2 concentration on gel polymerization. Inset: photographs of the polymerization system in response to different concentration of H_2O_2.

larger proteins. This observation aligned with the respective pore sizes of the two gels, with the traditional gel possessing smaller pores and the novel gel featuring larger pores. Unlike the control group, the HRP-catalyzed gel was easier to distinguish high molecular weight proteins within the same electrophoresis duration, suggesting that the pore size of the polyacrylamide gel formed through enzyme catalysis was different from that of the hydrogel prepared by TEMED/APS.

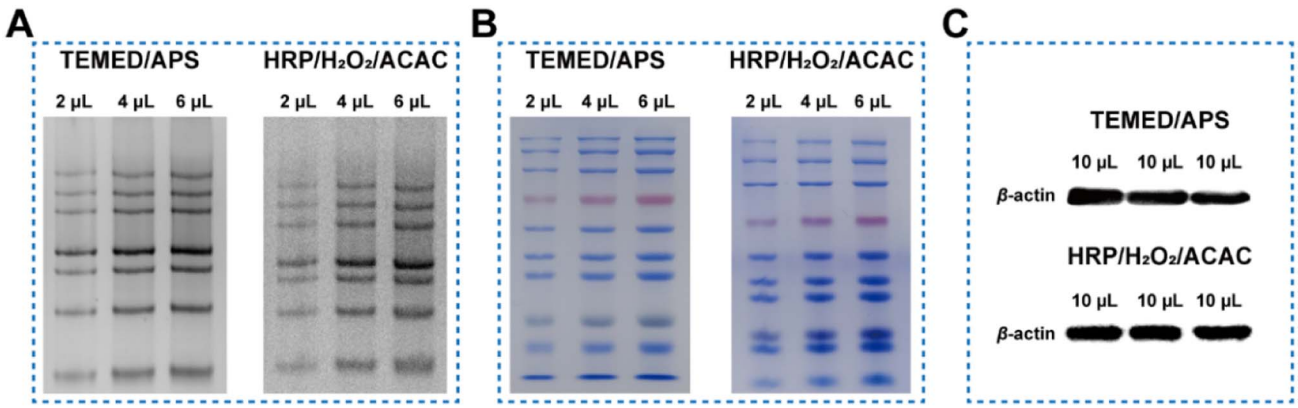

Fig. 4 **Verification of the electrophoretic function of polyacrylamide gels catalyzed by HRP/H_2O_2/ACAC.** Different concentration of DNA marker (A) and protein marker (B) were analyzed by performing electrophoresis using 10% polyacrylamide gels catalyzed by TEMED/APS (left) and HRP/H_2O_2/ACAC (right). (C) Western blot analysis of β-actin separated by the two kinds of polyacrylamide gel electrophoresis.

Additionally, we investigated whether the gel catalyzed by HRP would affect the subsequent transfer membrane and chemiluminescence imaging. Two types of gel electrophoresis were used to separate cell proteins, and then transferred to a PVDF membrane for autoradiography. The presence of a clear single protein band for β-actin indicated that HRP/H_2O_2/ACAC could completely replace TEMED/APS as the initiating system to catalyze the formation of polyacrylamide gels (Fig. 4C).

Conclusions

In this study, the HRP/H_2O_2/ACAC ternary system was employed as a substitute for TEMED/APS to facilitate the polymerization of Acr-Bis. The gel initiated by the HRP/H_2O_2/ACAC was confirmed to be capable of conducting functional experiments, such as protein and nucleic acid electrophoresis, which demonstrating its potential application in electrophoresis. In solution, the conversion of optical energy in AIE molecules leaded to heat dissipation, causing fluorescence quenching. Conversely, in the aggregated state, the movement of AIE molecules was constrained, thereby suppressing non-radiative decay mechanisms in the excited state. Consequently, the dissipation of energy through motion was diminished, while the emission of light was augmented, resulting in a substantial enhancement of fluorescence. The AIE property of BSA-Au NCs was utilized to monitor the kinetics of the polymerization reaction of Acr-Bis monomers. These findings would offer novel insights into the monitoring of polymerization systems and present an advanced strategy for investigating a secure catalytic system for gel polymerization.

Author contributions

Chang Liao: conceptualization; writing-original draft. Tao Li: validation; writing-original draft. Fengjiao Chen: funding acquisition; methodology. Shaoying Yan: funding acquisition; data curation. Liying Zhu: formal analysis. Hua Tang: writing – review; supervision; visualization. Dan Wang: writing – review; funding acquisition; project administration. The final draft of this paper was reviewed and approved by all authors.

Data availability

All data analyzed during this study are included in this published article.

Conflicts of interest

There are no conflicts to declare.

Acknowledgements

This study was supported by the Project funded by China Postdoctoral Science Foundation (2023MD734126), the National Natural Science Foundation of China (82060446), Medical Science and Technology Research Project of Henan Province (SBGJ202103110), and Jiangxi Provincial Natural Science Foundation (20212BAB206036). We would like to express our gratitude to all those who supported the subject.

References

1 A. Chrambach and D. Rodbard, Polyacrylamide gel electrophoresis, *Science*, 1971, **172**(3982), 440–451.
2 P. Menter, Acrylamide Polymerization-A Practical Approach, *Bio-Rad Tech Note*, 2000, **1156**, 24.
3 C. Pushparajan, S. K. Goswami, C. J. McAdam, *et al.*, A mechanically strengthened polyacrylamide gel matrix fully compatible with electrophoresis of proteins and nucleic acids, *Electrophoresis*, 2018, **39**(5–6), 824–832.
4 A. A. Al-Tubuly, SDS-PAGE and Western Blotting, *Methods Mol. Med.*, 2000, **40**, 391–405.
5 Q. Shi and G. Jackowski, One dimensional polyacrylamide gel electrophoresis, in *Gel electrophoresis of protein: a practical approach*, ed. B. D. Hames, Oxford University Press, Oxford, 1998, pp. 1–52.
6 Y. S. Kim, M. W. Baek, J. H. Sung, *et al.*, Acute and Subchronic Oral Toxicity Study of Ammonium Persulfate in Spraque-Dawley Rats, *Toxicol. Res.*, 2009, **25**(3), 132–139.
7 A. A. Fisher and A. Dooms-Goossens, Persulfate hair bleach reactions. Cutaneous and respiratory manifestations, *Arch. Dermatol.*, 1976, **112**(10), 1407–1409.
8 Y. Yue, T. Y. Liu, H. W. Li, *et al.*, Microwave-assisted synthesis of BSA-protected small gold nanoclusters and their fluorescence-enhanced sensing of silver (I) ions, *Nanoscale*, 2012, **4**(7), 2251–2254.
9 S. Pang and M. Z. Fiume, Final report on the safety assessment of Ammonium, Potassium, and Sodium Persulfate, *Int. J. Toxicol.*, 2001, 7–21.
10 M. Ahmed, N. Latif, R. A. Khan, *et al.*, Toxicological effect of *N,N,N′,N′*-tetramethylethylene on rat brain acetylcholinesterase, *Toxicol. Ind. Health*, 2014, **30**(5), 415–420.
11 M. Ahmed, M. R. C. Schetinger, J. B. T. Rocha, *et al.*, Toxicological effects of *N,N,N′,N′*-tetramethylethylenediamine on electric eel (Electrophorus electricus) acetylcholinesterase and human serum butyrylcholinesterase, *Toxicol. Environ. Chem. Rev.*, 2009, **91**(5–6), 1149–1157.
12 G. Parravano, Chain Reactions Induced by Enzymic Systems, *J. Am. Chem. Soc.*, 2002, **73**(1), 183–184.
13 A. E. Enciso, L. Fu, S. Lathwal, *et al.*, Biocatalytic "Oxygen-Fueled" Atom Transfer Radical Polymerization, *Angew. Chem., Int. Ed.*, 2018, **57**(49), 16157–16161.
14 A. Berberich Jason, *et al.*, Well-Defined Macromolecules Using Horseradish Peroxidase as a RAFT Initiase, *Macromol. Rapid Commun.*, 2016, **37**(4), 362–367.
15 S. Sen and J. E. Puskas, Green polymer chemistry: enzyme catalysis for polymer functionalization, *Molecules*, 2015, **20**(5), 9358–9379.
16 R. Li, W. Kong and Z. An, Controlling Radical Polymerization with Biocatalysts, *Macromolecules*, 2023, **56**(3), 751–761.
17 S. Zhu, X. Wang, Y. Cong, *et al.*, Free radical polymerization of gold nanoclusters and hydrogels for cell capture and light-

controlled release, *ACS Appl. Mater. Interfaces*, 2021, **13**(16), 19360–19368.
18 A. P. Danielson, D. B. Van-Kuren, J. P. Bornstein, *et al.*, Investigating the Mechanism of Horseradish Peroxidase as a RAFT-Initiase, *Polymers*, 2018, **10**(7), 741.
19 T. Lalot, M. Brigodiot and E. Maréchal, A kinetic approach to acrylamide radical polymerization by horse radish peroxidase-mediated initiation, *Polym. Int.*, 1999, **48**, 288–292.
20 J. W. Bae, J. H. Choi, Y. Lee, *et al.*, Horseradish peroxidase-catalyzed in situ forming hydrogels for tissue-engineering application, *J. Regener. Med. Tissue Eng.*, 2015, **9**(11), 1225–1232.
21 R. Derango, L. C. Chiang, R. Dowbenko, *et al.*, Enzyme-mediated polymerization of acrylic monomers, *Biotechnol. Tech.*, 1992, **6**, 523–526.
22 T. Su, D. Zhang, Z. Tang, *et al.*, HRP-mediated polymerization forms tough nanocomposite hydrogels with high biocatalytic performance, *Chem. Commun.*, 2013, **49**(73), 8033–8035.
23 S. T. Knox, S. Parkinson, R. Stone, *et al.*, Benchtop Flow-NMR for Rapid Online Monitoring of RAFT and Free Radical Polymerization in Batch and Continuous Reactors, *Polym. Chem.*, 2019, **10**(35), 4774–4778.
24 J. J. Haven and T. Junkers, Online Monitoring of Polymerizations: Current Status, *Eur. J. Org Chem.*, 2017, 6474–6482.
25 F. W. Wang, R. E. Lowry, W. J. Pummer, *et al.*, Fluorescence Monitoring of Viscosity and Chemical Changes During Polymerization, *ACS Symp.*, 1987, 454–462.
26 J. M. Nölle, C. Jüngst, A. Zumbusch, *et al.*, Monitoring of viscosity changes during free radical polymerization using fluorescence lifetime measurements, *Polym. Chem.*, 2014, 2700–2703.
27 J. Luo, Z. Xie, J. W. Lam, *et al.*, Aggregation-induced emission of 1-methyl-1,2,3,4,5-pentaphenylsilole, *Chem. Commun.*, 2001, 1740–1741.
28 J. Liu, H. Zhang, L. Hu, *et al.*, Through-Space Interaction of Tetraphenylethylene: What, Where, and How, *J. Am. Chem. Soc.*, 2022, **144**(17), 7901–7910.
29 H. Wang, E. Zhao, J. W. Y. Lam, *et al.*, AIE luminogens: emission brightened by aggregation, *Mater. Today*, 2015, 365–377.
30 J. Qian and B. Z. Tang, AIE Luminogens for Bioimaging and Theranostics: From Organelles to Animals, *Chem*, 2017, **3**(1), 56–91.
31 G. Niu, R. Zhang, X. Shi, *et al.*, AIE luminogens as fluorescent bioprobes, *TrAC, Trends Anal. Chem.*, 2019, **123**, 115769.
32 Z. Lei, J. Zhou, M. Liang, *et al.*, Aggregation-Induced Emission of Au/Ag Alloy Nanoclusters for Fluorescence Detection of Inorganic Pyrophosphate and Pyrophosphatase Activity, *Front. Bioeng. Biotechnol.*, 2021, **8**, 628181.
33 H. T. Sun and Y. Sakka, Luminescent metal nanoclusters: controlled synthesis and functional applications, *Sci. Technol. Adv. Mater.*, 2014, 506–512.
34 Y. Sun, T. Shu, J. Ma, *et al.*, Rational design of ZIF-8 for constructing luminescent biosensors with glucose oxidase and AIE-type gold nanoclusters, *Anal. Chem.*, 2022, 3408–3417.
35 W. Wang, Z. Wang, D. Sun, *et al.*, Supramolecular Self-Assembly of Atomically Precise Silver Nanoclusters with Chiral Peptide for Temperature Sensing and Detection of Arginine, *Nanomaterials*, 2022, **12**, 424.
36 Z. F. Pu, P. Jun, Q. L. Wen, *et al.*, Photocatalytic synthesis of BSA-Au nanoclusters with tunable fluorescence for highly selective detection of silver ion, *Dyes Pigm.*, 2021, 109533.
37 W. Zhu, H. Li and A. Wan, EDC-Induced Self-Assembly of BSA-Au NCs, *J. Fluoresc.*, 2019, **29**(3), 627–630.
38 J. Xie, Y. Zheng and J. Y. Ying, Protein-directed synthesis of highly fluorescent gold nanoclusters, *J. Am. Chem. Soc.*, 2009, **131**(3), 888–889.
39 A. Jyothikumar, M. Kailasnath, J. Simon, *et al.*, BSA Stabilized Gold Nanoparticles: Synthesis and Characterization, *Mater. Today: Proc.*, 2019, **9**, 111–115.
40 T. Wang and D. Xiao, Rapid synthesis of fluorescent bovine serum albumin-gold nanoclusters complex for glutathione determination, *Mikrochim. Acta*, 2021, **188**(6), 193.
41 Z. Tan, H. Xu, G. Li, *et al.*, Fluorescence quenching for chloramphenicol detection in milk based on protein-stabilized Au nanoclusters, *Spectrochim. Acta, Part A*, 2015, **149**, 615–620.
42 T. Shu, L. Su, J. Wang, *et al.*, Chemical etching of bovine serum albumin-protected Au25 nanoclusters for label-free and separation-free detection of cysteamine, *Biosens. Bioelectron.*, 2015, **66**, 155–161.
43 C. W. Wang, Y. N. Chen, B. Y. Wu, *et al.*, Sensitive detection of cyanide using bovine serum albumin-stabilized cerium/gold nanoclusters, *Anal. Bioanal. Chem.*, 2016, **408**(1), 287–294.
44 Y. Xu, P. Zhang, Z. Wang, *et al.*, Determination of the activity of telomerase in cancer cells by using BSA-protected gold nanoclusters as a fluorescent probe, *Mikrochim. Acta*, 2018, **185**(3), 198.
45 N. Y. Hsu and Y. W. Lin, Microwave-assisted synthesis of bovine serum albumin-goldnanoclusters and their fluorescence-quenched sensing of Hg^{+} ions, *New J. Chem.*, 2016, **40**, 1155–1161.
46 R. Jin, C. Zeng, M. Zhou, *et al.*, Atomically Precise Colloidal Metal Nanoclusters and Nanoparticles: Fundamentals and Opportunities, *Chem. Rev.*, 2016, **116**(18), 10346–10413.
47 C. Ding, Y. Xu, Y. Zhao, *et al.*, Fabrication of BSA@AuNC-Based Nanostructures for Cell Fluoresce Imaging and Target Drug Delivery, *ACS Appl. Mater. Interfaces*, 2018, **10**(10), 8947–8954.
48 I. Fabijanić, M. Jurković, D. Jakšić, *et al.*, Photoluminescent Gold/BSA Nanoclusters (AuNC@BSA) as Sensors for Red-Fluorescence Detection of Mycotoxins, *Materials*, 2022, **15**(23), 8448.
49 S. Govindaraju, S. R. Ankireddy, B. Viswanath, *et al.*, Fluorescent Gold Nanoclusters for Selective Detection of Dopamine in Cerebrospinal fluid, *Sci. Rep.*, 2017, **7**, 40298.

50 Z. Tang, F. Chen, D. Wang, *et al.*, Fabrication of avidin-stabilized gold nanoclusters with dual emissions and their application in biosensing, *J. Nanobiotechnol.*, 2022, **20**(1), 306.
51 S. Pang, A ratiometric fluorescent probe for detection of uric acid based on the gold nanoclusters-quantum dots nanohybrid, *Spectrochim. Acta, Part A*, 2019, **222**, 117233.
52 P. Bukackova, Mathematical Methods in the Calculation of the Zeta Potential of BSA, *J. Solution Chem.*, 2018, **47**, 1942–1952.
53 Z. Tang, F. Chen, D. Wang, *et al.*, Fabrication of avidin-stabilized gold nanoclusters with dual emissions and their application in biosensing, *J. Nanobiotechnol.*, 2022, **20**(1), 306.
54 L. Luo and R. Jin, Atomically precise metal nanoclusters meet metal-organic frameworks, *iScience*, 2021, **24**(10), 103206.
55 N. Tarasova, A. Zanin, E. Krivoborodov, *et al.*, The New Approach to the Preparation of Polyacrylamide-Based Hydrogels: Initiation of Polymerization of Acrylamide with 1,3-Dimethylimidazolium (Phosphonooxy-)Oligosulphanide under Drying Aqueous Solutions, *Polymers*, 2021, **13**(11), 1806.
56 W. Xie, L. Zhao, Y. Wei, *et al.*, Advances in enzyme-catalysis-mediated RAFT polymerization, *Cell Rep. Phys. Sci.*, 2021, 100487.
57 R. Wang, L. Rong, S. Ni, *et al.*, Enzymatic graft polymerization from cellulose acetoacetate: a versatile strategy for cellulose functionalization, *Cellulose*, 2021, **28**(2), 1–11.